Available online at www.sciencedirect.com
ScienceDirect
Geochimica et Cosmochimica Acta 70 (2006) 5285–5292
Geochimica
www.elsevier.com/locate/gca

A simple model for the effect of hydration on the distribution of ferrous iron at reduced hematite (0 1 2) surfaces

Jianwei Wang, James R. Rustad *

Department of Geology, University of California, Davis, One Shields Avenue, Davis, CA 95616, USA

Received 18 January 2006; accepted in revised form 10 August 2006

Abstract

Using a simple ionic model with polarizable oxygen ions and dissociating water molecules, we have calculated the energetics governing the distribution of Fe(II)/Fe(III) ions at the reduced (2×1) surface of α-Fe_2O_3 (hematite) (0 1 2) under dry and hydrated conditions. The results show that systems with Fe(II) ions located in the near-surface region have lower potential energy for both dry and hydrated surfaces. The distribution is governed by coupling of the ferrous iron centers to positive charge associated with missing oxygen atoms on the dry reduced (2×1) (0 2 1) surface. As the surface is hydroxylated, the missing oxygen rows are filled and protons from dissociated water molecules become the positive charge centers, which couple more weakly to the ferrous iron centers. At the same time, the first-layer iron centers change from fourfold or fivefold coordination to sixfold coordination lowering the potential energy of ferric iron in the first layer and favoring migration of ferrous iron from the immediate surface sites. This effect can also be understood as reflecting stronger solvation of Fe(III) by the adsorbed water molecules and by hydrolysis reactions favoring Fe(III) ions at the immediate surface. The balance between these two driving forces, which changes as a function of hydration, provides a compelling explanation for the anomalous coverage dependence of water desorption in ultra-high vacuum experiments.
© 2006 Elsevier Inc. All rights reserved.

1. Introduction

Hematite (α-Fe_2O_3) is the most stable iron oxide at the Earth's surface and is abundant in natural environments (Cornell and Schwertmann, 1996). Work over the last decade has focused on its interaction with water (Wasserman et al., 1997; Henderson et al., 1998; Parker et al., 1999; Rustad et al., 1999; Jones et al., 2000; Henderson, 2002; Trainor et al., 2004) and electron transfer across mineral-water interfaces (Eary and Rai, 1989; Eggleston, 1999; Jeon et al., 2003; Williams and Scherer, 2004; Madden and Hochella, 2005). It has been shown that the reduction of U(VI) (Liger et al., 1999), Tc(VII) (Lloyd et al., 2000; Fredrickson et al., 2004), and nitrobenzene (Williams and Scherer, 2004) by ferrous ions is dramatically enhanced by the presence of hematite particles in aqueous solutions. Oxidation–reduction processes taking place at hematite surfaces are believed to involve small amounts of ferrous iron dissolved in nominally Fe^{3+} oxide (Eary and Rai, 1989). The question of the structural arrangement of Fe(II) on Fe(III) oxide surfaces is thus central to understanding iron oxide reactivity.

Ultra-high vacuum (UHV) experiments on the behavior of water on reduced hematite (0 1 2) surfaces provide a well-defined benchmark for understanding the driving forces governing Fe(II)–Fe(III) distributions at iron oxide surfaces (Henderson et al., 1998). In UHV environments, the hematite (0 1 2) surface has been shown to exist in two stable oxidation states. The stoichiometric (1×1) state undergoes a (2×1) reconstruction upon heating in UHV conditions above 900 K. This reconstruction is driven by the emission of O_2 and the generation of oxygen vacancies and Fe(II) ions produced by the electrons left behind by the oxygen gas (Gautier-Soyer et al., 1996). Henderson et al. (1998) examined the chemisorption of water on the reduced (2×1) surface. They showed that the temperature-pro-

* Corresponding author. Fax: +1 530 752 0951.
E-mail address: rustad@geology.ucdavis.edu (J.R. Rustad).

0016-7037/$ - see front matter © 2006 Elsevier Inc. All rights reserved.
doi:10.1016/j.gca.2006.08.022

grammed desorption of water exhibited anomalous and complex coverage dependence. We hypothesize that the complexity observed in the experiments of Henderson et al. (1998) results from changes in the surface distribution Fe(II)–Fe(III) as a function of water coverage. To test this hypothesis, we calculate the relative energies of different Fe(II)–Fe(III) arrangements within slab models of the hematite surface, and ascertain the effect of surface hydration on these energies.

2. Methods

2.1. Structure and construction of the model surface

The (0 1 2) surface of hematite has two oxidation states (Henderson et al., 1998) [the right-hand convention is used here to index the lattice planes, see Henderson et al. (1998) for discussion of the various conventions in the literature]. Under UHV conditions, the (1×1) surface is fully stoichiometric and has a bulk-terminated structure (Henrich and Cox, 1994) with fivefold coordinated Fe(III) at the surface. This surface can be prepared by oxidation of natural hematite at $P_{O_2}=10^{-6}$ mbar and 700 K (Gautier-Soyer et al., 1996). After annealing ($P_{O_2}=10^{-10}$ mbar) at temperature 900 K, the (0 1 2) surface showed a (2×1) LEED pattern, indicating surface reconstruction (Gautier-Soyer et al., 1996; Henderson et al., 1998; Lad and Henrich, 1988). The exact atomic structure of reconstructed (2×1) surface remains unknown, however, high resolution electron energy loss (HREELS) and Auger spectra have shown that the surface has reduced Fe(II) ions (Henderson et al., 1998). The similarity of the HREELS spectra of the (1×1) and (2×1) surfaces suggested that the near-surface regions are terminations of the hematite structure.

We model the surface as a 2D periodic slab cut from bulk hematite structure parallel to (0 1 2), with supercell dimensions in the surface plane fixed at the optimized bulk values of 10.28 Å and 5.51 Å. These dimensions reflect the minimum dimensions of the (2×1) surface cut from the bulk optimized within the potential used here (Fig. 1a). Each iron layer has four iron atoms. The surface slab consists of a total of 10 iron ion layers (25 atomic layers) with a total thickness of ~17.5 Å (Fig. 1b). This slab is thicker than the stoichiometric slabs required for model convergence in previous studies (Wasserman et al., 1997, 1999). The inversion symmetry present in bulk hematite was enforced in the slab to eliminate any ferroelectric response in the (0 0 1) direction. The dimension of the cell normal to the surface was set to 100 Å to prevent interactions between the two surfaces when applying three-dimensional periodic boundary conditions. A smaller spacing may be possible but this was not investigated. A total of four Fe(II) ions were introduced in the system to replace Fe(III) ions, and one oxygen atom was removed from the top and bottom surface, as indicated in Figs. 1a and 2a. In the hydrated state, water molecules fill the surface oxygen vacancies on the top and bottom of the slab. Water molecules are also adsorbed on the surface iron atoms (four on top and four on the bottom) (Fig. 2b). There are therefore 10 water molecules (five on top and five on the bottom) added per each (2×1) unit cell indicated in Fig. 1a.

2.2. Interaction potentials

A review of the testing and development of the potential set may be found in Rustad (2001). A few relevant points are restated here. The Fe–O potential parameters were fitted to ab initio calculations of the Fe^{3+}-H_2O potential surface of Curtiss et al. (1987). The O–O and O–H interactions are those of the polarizable, heterolytically dissociative water model of Halley et al. (1993). Solid-state data were not used to any extent in the parameterization process. Despite this, very good agreement was obtained for surface relaxation as a function of depth on vacuum-terminated hematite (0 0 1) surfaces as measured with X-ray photoelectron diffraction (Rustad, 2001 and references therein). Both the **a** and **c** parameters of optimized bulk hematite are within 3% of experimental values (5.14 Å and 13.91, compared with the experiment of 5.03 and 13.75 Å) (Waychunas, 1991). A similar level of agreement is obtained for the FeOOH polymorphs and Fe(II)-containing minerals such as magnetite (Rustad, 2001 and references therein). The potentials have also been used extensively for monomeric (Fe^{2+}, Fe^{3+}; Rustad et al., 1995, 2004) and multimeric species (Fe^{3+}) in aqueous solution, including hydrolysis species. The potentials were also instrumental in the interpretation of UHV experiments the interaction of water with the hematite (0 1 2) surface (Henderson et al., 1998). These simply constructed potentials give quite reasonable results for Fe^{2+}, Fe^{3+}–H_2O, OH^-, O^{2-} and have been successfully applied to a wide range of problems in mineralogy, high-vacuum surface science, and interfacial chemistry, including problems involving the pH-dependence of rates of electron transfer (Rustad, 2001 and references therein; Rustad et al., 2003, 2004).

Formal charges are used for all species in the model along with polarizable oxygen anions. The point dipole μ_i on the oxygen atom self-consistently satisfies the relation $\mu_i=\alpha E_i$, where E_i is the electric field at the oxygen and α is the oxide ion polarizability, set to 1.444 $Å^3$. The cation-oxygen charge–dipole interactions at short distance are screened through multiplication by a cutoff function (the same for the Fe(II) and Fe(III) ions), having a value of zero at small distance and unity at large distance.

This work makes the approximation that Fe(II)–Fe(III) charges are well localized. Prediction of the extent of charge localization in these and similar systems is an area of ongoing research and appears to be a sensitive function of the theoretical method used. Goethite, for example, is metallic in the generalized gradient approximation of density functional theory (R. Pentcheva, personal communication). Experimentally, it has been established that the effective Verwey transition temperature of magnetite is much higher for a surface than in the bulk (Wiesendanger

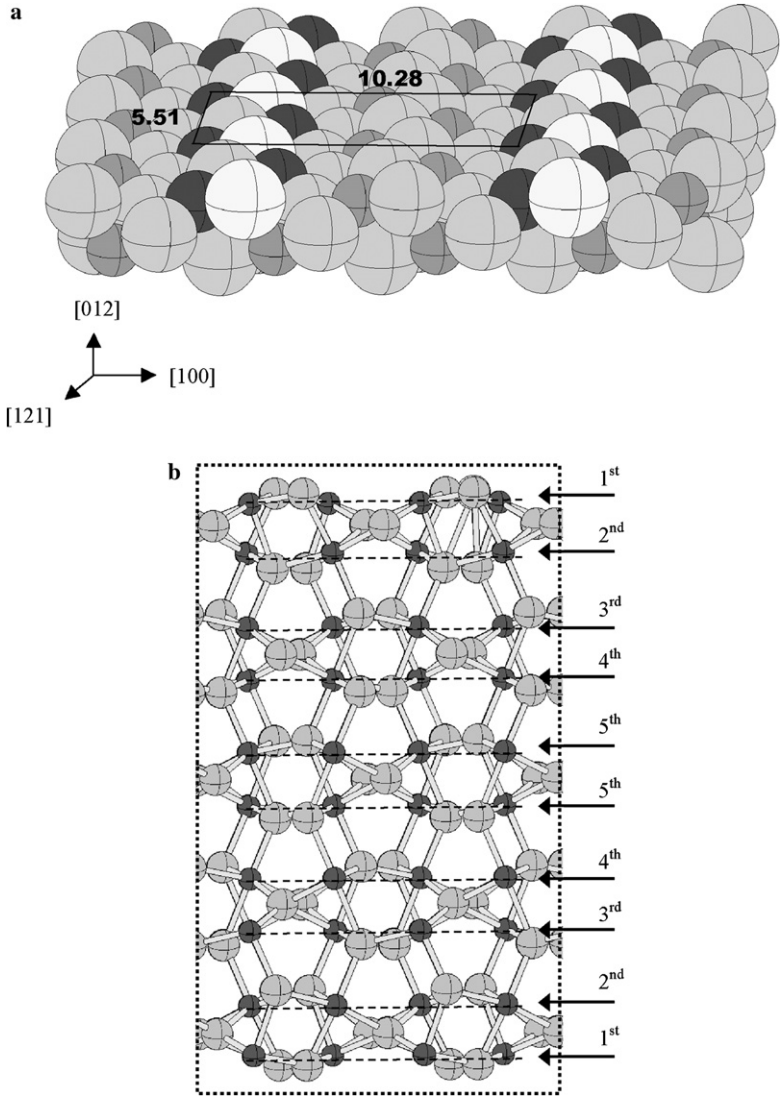

Fig. 1. (a) Schematic model of the bulk terminated hematite (α Fe_2O_3) (2×1) (0 1 2) surface. Larger spheres are oxygen atoms. The more lightly shaded oxygens are removed from the surface; the more darkly shaded oxygen atoms remain. Small dark spheres are Fe(II) ions which have the electrons left behind during removal of oxygen; smaller, lighter spheres are Fe(III) ions. The surface lattice unit for (2×1) surface is highlighted with the dimensions of 10.28 Å and 5.51 Å. (b) Computational (0 1 2) surface supercell in [0 1 2] and [1 0 0]. Arrows show the different Fe layers.

et al., 1994), so it may be that the localized-charge representation is a reasonable approximation in a surface environment. In any case, the localized charge arrangement serves as a useful end member in the interpretation of mixed-valence oxide surfaces.

2.3. Simulation procedures and analysis

Energy optimizations were performed for the reduced (2×1) surfaces by searching over all possible distributions of Fe(II) and Fe(III) ions under both hydrated and dry conditions. The initial atomic positions were set to those of the relaxed (unreduced) (0 1 2) surface. Previous work indicated negligible effects from the artificial periodic dimension normal to the slab, provided there is no overall dipole moment and provided the slabs are neutral (Wasserman et al., 1999). We therefore used the simpler three-dimensionally periodic Ewald summation for the charge–charge, charge–dipole, and dipole–dipole interactions (deLeeuw et al., 1980). The conjugate-gradient algorithm was used in energy minimization. All atomic positions and induced dipoles are fully optimized; the only constraints are the **a** and **b** vectors representing the surface unit mesh which are fixed at bulk values. For each surface, two sites out of 20 Fe atoms in the top half of the slab were designated to be Fe(II). These are repeated through the inversion operation in the lower half of the slab, resulting a total of 190 ($=20\times19/2!$)combinations for which energies were computed.

One of the important contributions to the slab energy is the effective electrostatic repulsion between the Fe(II) ions and their attraction to the surface defect (oxygen vacancy or adsorbed protons) to which the Fe(II) ions are coupled. Because of the inversion constraint, the concentration of

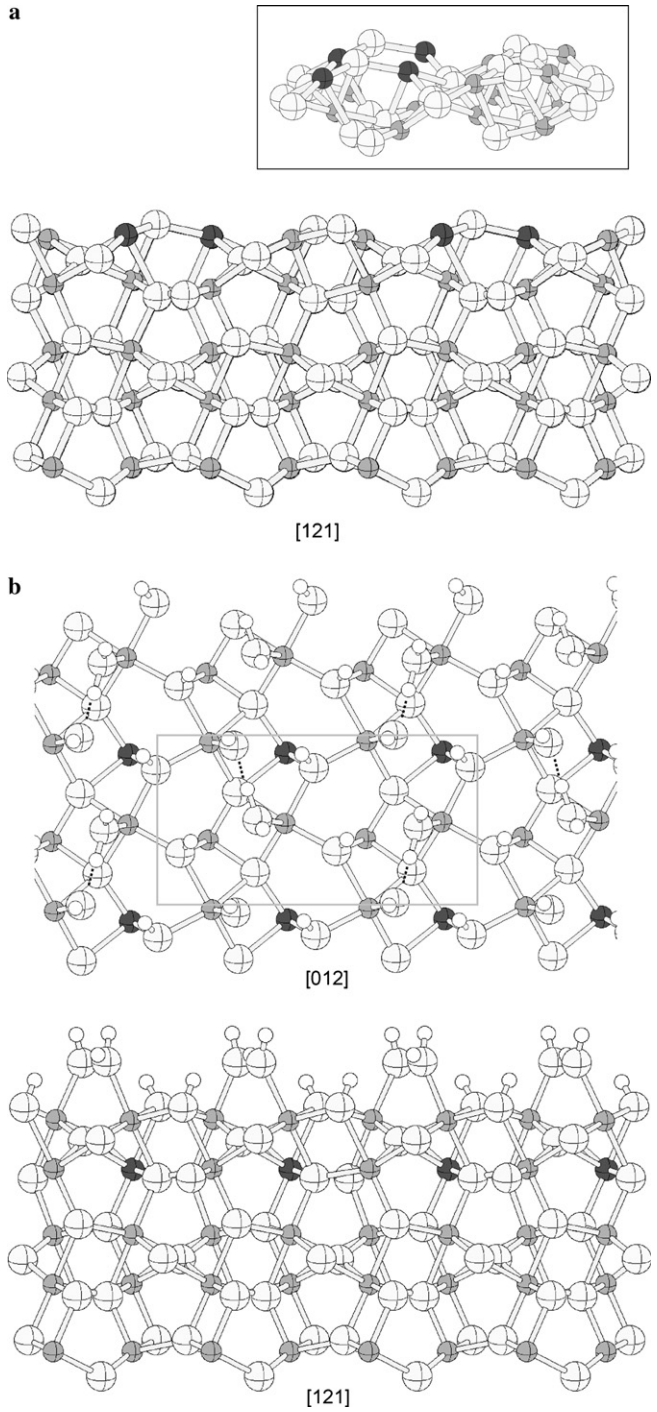

Fig. 2. Low-energy conformers (2 × 1) surface of (a) vacuum-terminated and (b) hydrated hematite (0 1 2) surface. The larger spheres are oxygen atoms, the intermediate-sized spheres are light (Fe^{3+} ions), dark (Fe^{2+} ions. The small, unfilled spheres are hydrogen ions. In (a), the inset shows the octahedral (90° and 180°) O–Fe(II)–O angles. For the vacuum-terminated surface the Fe(II) atoms remain directly at the surface sites. In (b) the top panel is normal to (0 1 2); the bottom cross-sectional panel is along [1 2 1]. In the hydrated surface, the Fe(II) ions have moved into the 2nd layer. Dashed lines indicate strong hydrogen bonds within $H_3O_2^-$ surface groups.

Fe(II) ions is far from the dilute limit of an infinitely thick slab, and the artificial interaction between Fe(II) ions across the slab will interfere to some extent with that between Fe(II) ions and rest of the surface. We have tried to minimize such effects by choosing a relatively thick slab. Since the coupling is the same for hydrated surface and dry surface, the comparison between these two systems is not, to first order, affected by this coupling.

3. Results

3.1. Structure of the low-energy surfaces

The lowest-energy structures for both the vacuum-terminated and hydrated surfaces are shown in Figs. 2a and b, respectively. The vacuum-terminated surface is consistent with the observed (2 × 1) structure and has the Fe(II) sites in fourfold coordination, but, as shown in the inset in Fig. 2a, the Fe(II) remains in nearly octahedral geometry; O–Fe(II)–O angles are close to 90° and 180°. The hydrated surface in Fig. 2b has the oxygen vacancies filled in by adsorbed water molecules, which have dissociated to completely fill the "zig-zag" surface oxygen rows with OH ions. The adsorbed water molecules have also dissociated on the (2 × 1) surface, forming infinite $–H_2O–OH–H_2O–$ chains along [1 2 1]. The dissociation is consistent with previous experimental investigations of Henderson et al. (1998). As can be seen in Fig. 2b, hydration of the surface drives the Fe(II) sites from the surface layer into the second layer. The low energy configuration for the hydrated surface is (1 × 1) with respect to the Fe(II)–Fe(III) distribution. This prediction is in disagreement with low-energy electron diffraction experiments in Henderson et al. (1998), where it was found that the (2 × 1) structure persisted from zero water coverage to coverages exceeding one monolayer. This is possibly a deficiency in the model, or may also reflect anisotropy in electron transfer rates in hematite (Iordanova et al., 2005). It is important to keep in mind that this paper does not deal with kinetics, only with equilibrium structure.

3.2. Slab energies

The parameterized model gives a good description of the structural relaxation and energetics of vacuum-terminated hematite (0 0 1) (Rustad, 2001). For example, the surface energy of the (0 0 1) slab is predicted to be 1.64 J/m^2, as compared with first-principles calculations of 1.52 J/m^2 (Wang et al., 1998). This is a small difference relative to the unrelaxed energy of 4.24 J/m^2. The predicted (1 × 1) hematite (0 1 2) surface energy is 2.0 J/m^2. As yet, there are no first principles calculations to compare this against.

The hydration energy is defined as:

$$[E^{\mathrm{hyd}}_{\mathrm{slab}} - (E^{\mathrm{dry}}_{\mathrm{slab}} + nE_{\mathrm{H_2O}})]/2A \quad (1)$$

where $E^{\mathrm{hyd}}_{\mathrm{slab}}$ is the energy of the hydrated slab, $E^{\mathrm{dry}}_{\mathrm{slab}}$ is the energy of the dry slab, $E_{\mathrm{H_2O}}$ is the energy of a gas-phase water molecule, A is the surface area, and n is the number of water molecules added to the slab (10 in this case). The hydration energy of the lowest-energy hydrated slab in

Fig. 2b is -5.2 J/m^2, much higher than the hydration energy of the stoichiometric (1×1) surface of hematite (0 1 2), -3.0 J/m^2, calculated using the same atomic interaction parameters (Rustad et al., 1999). The fact that, for the (1×1) surface, the hydration energy is greater than the surface energy simply indicates the metastability of hematite + water relative to goethite or $Fe(OH)_3$. Negative surface energies in oxide systems have been discussed in Wasserman et al. (1997) (iron oxide) and Lodziana et al. (2004) (alumina).

The higher hydration energy for the reduced (0 1 2) surface obtained here is qualitatively consistent with the temperature programmed desorption (TPD) experiments for water on stoichiometric (1×1) and reduced (2×1) surfaces (Henderson et al., 1998). The highest desorption peak observed on the (2×1) (0 1 2) surface is about 405 K at monolayer coverages. On the stoichiometric (1×1) surface, this peak is at 350 K (independent of coverage), indicating stronger hydration of the reduced surface. Both desorption peaks have been shown to result from recombination of dissociated adsorbed water. At the stoichiometric (1×1) surface, the oxygen atom of the dissociated adsorbed water molecule is coordinated to only one surface Fe(III) ion. At the reduced (2×1) surface, however, the oxygen atom of the dissociated adsorbed water molecule occupies the surface oxygen vacant site and is coordinated to three Fe ions (Fig. 2b). The higher desorption peak at the reduced surface is related to a different recombination of a H and an OH to form a H_2O, which needs to detach from three Fe ions while it only needs to detach from one Fe(III) ion at the (1×1) surface.

The slab energy as a function of the average z coordinate of the ferrous iron, $\bar{z}$, is shown in Fig. 3. Each point on this curve represents one of the 190 possible Fe(II)–Fe(III) distributions (some are the same by symmetry). For the dry surface, the minimal potential energy shows no minimum; the Fe(II) is predicted to lie directly on the surface as in Fig. 2a. For the hydrated surface, E vs $\bar{z}$ decreases more rapidly, and has a minimum around $\bar{z}=3.4$ (two Fe(II) atoms in the second layer from the top), as in Fig. 2b.

These results support our hypothesis that the anomalous coverage dependence of the water TPD experiments are due to rearrangements of the Fe(II)–Fe(III) ion distributions in response to increasing hydration. One of the important observations made in that study was that the main TPD peak at 405 K (at monolayer coverage) decreases with decreasing water coverage. This observation was puzzling because TPD peaks typically *increase* in temperature with decreasing water coverage in dissociative adsorption, as recombination is inhibited at low coverages. Our results suggest the following interpretation: The dry (2×1) surface has the ferrous iron confined to the first layer. As the surface hydrates, a minimum develops in the E vs $\bar{z}$ curve, moving some ferrous iron off the immediate surface into the second layer. The presence of this minimum results in a slight enrichment of ferric iron in the top layer, giving rise to stronger water binding for higher coverages.

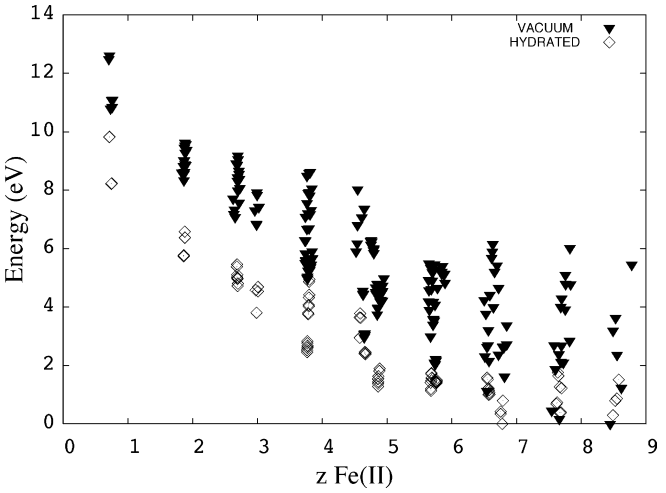

Fig. 3. The energy of the vacuum (upside-down triangles) and hydrated (open diamonds) surface as a function of the average position of the Fe(II) ions, $\bar{z}$, measured from the center of the slab. Energies are calculated relative to the lowest-energy surface for the hydrated states as shown in Fig. 2 (and, are therefore zero by definition for the slabs in Fig. 2. For the hydrated surface, the minimum-energy surface has $\bar{z}=6.8$ Å, while for the vacuum-terminated surface, the minimum-energy surface is close to $\bar{z}=8.4$ Å.

3.3. Normal mode analysis of the low energy structures

A normal mode analysis was carried out on (2×4) supercells representing the low-energy structures in Fig. 4. The normal mode analysis was carried out by diagonalization of the dynamical matrix calculated from finite difference using the forces evaluated with the conjugate gradient code. Starting from the optimized structure, each atom was moved forward and backward 0.001 Å and a finite difference of the forces was taken, allowing the polarization degrees of freedom to completely relax. The three eigenvectors representing translational motion of the lattice had associated frequencies less than 7 cm^{-1}. No negative eigenvalues were found; the structures therefore appear to be stable. The vibrational density of states was constructed by accumulating the observed frequencies (2301 frequencies for the vacuum-terminated surface and 3166 frequencies for the hydrated surface) into histograms about 10 cm^{-1} in resolution.

The force field has not been tested very thoroughly for vibrational frequencies. As a crude benchmark, consider the symmetric stretch mode of $Fe(H_2O)_6{}^{3+}$. The model predicts 614 cm^{-1}, 100 cm^{-1} higher than the experimentally observed frequency of approximately 500 cm^{-1}. While it is difficult to resolve anything definitive in the low frequency range of either the reduced or hydrated surface, it is worthwhile to point out some interesting features of the hydrated surface in the mid-range bands. The band at 1300 cm^{-1} is due to the δ-modes involving Fe–O–H bending in Fe_3OH groups. The modes at 1670–1730 and the

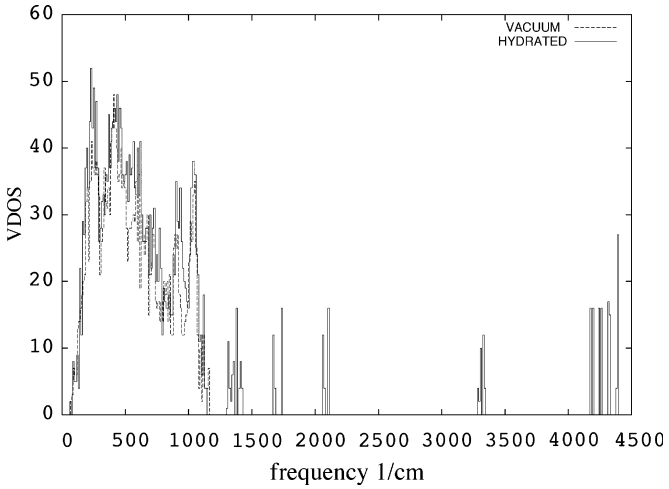

Fig. 4. Vibrational density of states evaluated for a (2×4) supercell of hydrated (solid) and vacuum-terminated (dashed) surfaces. The vibrational frequencies (2349-vacuum) and (3069-hydrated) were accumulated into bins approximately 10 cm^{-1} in width to obtain the vibrational density of states shown in the figure.

rather surprising intensity at 2050–2100 cm^{-1} is due to H–O–H wagging and bending motions, respectively, for Fe–(OH_2)–(OH)Fe groups—essentially $H_3O_2^-$ groups adsorbed at the surface. To check these predictions, an electronic structure calculation was carried out on $(H_2O)_4Al(\mu\text{-}OH)_2Al(OH)(H_2O)_3^{3+}$ using B3LYP and 6-31G*, having an HO–HOH moiety similar to those observed in our force field calculations on the surface. The frequency of the H–O–H bending motion for the (Al)–HO ↔ HOH–(Al) group is 1957 cm^{-1}, indicating that our calculations are in a reasonable range. There are no obvious features in this range in the HREELS spectrum of the hydrated (2×1) surface measured by Henderson et al. (1998). On the other hand, there was abundant evidence for water dissociation on this surface, which would presumably indicate the presence of HO–OH_2 groups on the surface. It is possible that the HREELS signal of these groups is small, but the discrepancy warrants further investigation. To our knowledge, the usefulness of this frequency band, potentially diagnostic for water dissociation on oxide surfaces, has not been previously recognized. The frequencies at 3300 cm^{-1} are HO–H stretching motions within the $H_3O_2^-$ groups at the surface, and those above 4200 cm^{-1} are the free-OH stretches.

4. Discussion

Several factors are expected to influence the distribution of ferrous iron on the (2×1) surface. First, there is the electrostatic interaction between Fe(II) ion sites and the missing oxygen atoms producing the O_2 gas emitted from the surface. Relative to Fe(III) the reduced Fe(II) act like negatively charged sites, carrying an additional electron. At the dry surface, the missing oxygen atoms leave a net positive charge relative to the occupied surface oxide sites. The electrostatic interaction between the "negatively charged" Fe (II) sites and the "positively charged" missing oxygen rows, of course, binds the Fe(II) ions to the surface.

A second factor concerns the fourfold and fivefold coordination of the surface iron sites on the dry (2×1) surface. All else being equal, the reaction:

$$^{IV}Fe(III) + {}^{V}Fe(\ II) = {}^{V}Fe(III) + {}^{IV}Fe(II) \qquad (2)$$

should be favored: there are four strong Fe(III)–O bonds on the left and five on the right. In a restricted surface environment, where the Fe center remains octahedral, the Fe(II) ions should partition into the lower-coordinated sites. The picture would change if the sites converted to tetrahedral geometry with shorter Fe–O bonds. For example, in comparing the energies of Fe(II) and Fe(III) for different sites in magnetite, our model does in fact give preference to the inverse structure with Fe^{3+} in the tetrahedral sites, [see Rustad (2001)]). However, the coordination geometry of the Fe(II) sites is maintained in our calculations (see Fig. 2a), and also seems supported by HREELS data of Henderson et al. (1998), which were consistent with the (2×1) surface being a termination of the hematite structure.

Hydroxylation of the surface changes both of these factors. As the surface is covered with water molecules, the positively charged oxygen vacancies are filled in with oxide ions from water molecules. The compensating charge is then associated with protons that dissociate from the water molecules filling in the missing row on the dry surface. These protons ultimately end up binding to triply coordinated surface oxide ions to form OH^- ions. In effect, the positive charge associated with the missing oxide ions on the dry surface has migrated to "extra" protons adsorbed to the hydroxylated surface. It is interesting to ask how this might affect the E vs $\bar{z}$ curve. Does the ferrous iron couple more strongly to the protons or to the oxygen vacancies? Does hydroxylation, which also converts the fourfold or fivefold surface sites to sixfold surface sites, eliminate the contribution from Eq. (2)?

Our calculations suggest two things. First, the overall E vs $\bar{z}$ curve is lower for the hydroxylated system than the vacuum system; the ferrous irons appear to couple less strongly to the protons than to the oxygen vacancies. This may be due to the fact that the ferrous iron can get closer to the oxygen vacancies than to the protons. More striking, however, is that completing the coordination shells of the surface ions by adsorbed water molecules appears to have forced the ferrous iron into the second layer. This is in part due to the elimination of the fivefold coordinated sites as the surface is hydroxylated. This might also be looked at as a solvation or acid–base effect; to the extent that the adsorbed water acts like a dielectric solvent, a more favorable solvation contribution will come from the Fe(III)–H_2O interaction than from the Fe(II)–H_2O interaction. The enhanced acidity of the Fe(III)–OH_2 groups will drive the reaction in the same way because

there is potential energy to be gained from dissociation of surface functional groups.

5. Geochemical implications

Our results, which employ the simplest possible molecular model, provide a compelling interpretation of the experiments of Henderson et al. (1998) , and highlight the significance of that work for geochemistry. One important point, often overlooked, is that motion of the "extra" electrons associated with the ferrous iron must be coupled to positive charges somewhere else. It is clear that ferrous iron ion will not migrate into the solid without taking these charges with them. In the case of the dry UHV experiments, these are oxygen vacancies. For hydrated surfaces, the ferrous iron is coupled to proton positions. In geochemical contexts, the hydrated surface is relevant, and the migration of electron charge is likely to be associated with the mobility of protons into the lattice. The reorganization energies associated with the motion of surface protons into the bulk are likely to be larger than the reorganization energies associated with the transfer of electrons, and are probably rate-limiting.

The overall interaction between the ferrous iron and the localized proton charge centers (on the hydroxylated surface) is somewhat weaker than between the ferrous iron and the positive charge associated with oxygen vacancies (on the dry surface). For the hydrated surface, the existence of a minimum in the energy for configurations in which ferrous iron ions move off the immediate surface sites indicates that the ferrous iron may be buried slightly below the immediate surface in the presence of water. These near-surface rearrangements, driven by solvation forces and acid–base reactions, appear to be rapid, since the electrons appear to redistribute on the hour-long time scales associated with the TPD experiments, having an important influence on the chemical behavior of surface water. The relatively fast kinetics associated with the near-interfacial burial of ferrous iron are consistent with the oxidation of sorbed Fe(II) to Fe(III) at iron oxide/oxyhydroxide surfaces observed by Williams and Scherer (2004) in Moessbauer studies. These results also have implications for the recently discovered catalytic effect of Fe(II) on solid-state Fe-oxide transformations (Pedersen et al., 2005). Migration of Fe(II) into the bulk weakens foundational bonds, and is likely to enhance lability, and aid structural reorganization.

The structural state of adsorbed Fe(II) will differ from the idealized configurations in the UHV systems, but the factors governing the behavior of these sorbed ions are likely to be similar to the factors we have identified in our analysis of the UHV experiments. The driving forces uncovered by the ionic model presented here are fundamental; additional sophistication, such as could be achieved with methods based on electronic structure, are unlikely to change this first-order picture, which will serve as an important boundary condition to the details of the ultimate electronic response of the system.

Acknowledgments

This research was supported by the US D.O.E., Office of Basic Energy Sciences division of the U.S. DOE (DE-FG02-05ER15639 to JRR) and by the National Science Foundation (EAR -0515600).

Associate editor: David R. Cole

References

Cornell, R.M., Schwertmann, U., 1996. *The Iron Oxides: Structure, Properties, Reactions, Occurrence and Uses*. VCH, New York.

Curtiss, L.A., Halley, J.W., Hautman, J., Rahman, A., 1987. Nonadditivity of ab-initio pair potentials for molecular dynamics of multivalent transition metal ions in water. *J. Chem. Phys.* **86**, 2319–2327.

deLeeuw, S.W., Perram, J.W., Smith, E.R., 1980. Simulation of electrostatic systems in periodic boundary-conditions: 1. Lattice sums and dielectric-constants. *Proc. R. Soc. London, A-Math., Phys., Eng. Sci.* **373**, 27–56.

Eary, L.E., Rai, D., 1989. Kinetics of chromate reduction by ferrous-ions derived from hematite and biotite at 25 °C. *Am. J. Sci.* **289**, 180–213.

Eggleston, C.M., 1999. The surface structure of α-Fe_2O_3 (001) by scanning tunneling microscopy: implications for interfacial electron transfer reactions. *Am. Mineral.* **84**, 1061–1070.

Fredrickson, J.K., Zachara, J.M., Kennedy, D.W., Kukkadapu, R.K., McKinley, J.P., Heald, S.M., Liu, C., Plymale, A.E., 2004. Reduction of TcO_4^- by sediment-associated biogenic Fe(II). *Geochim. Cosmochim. Acta* **68** (15), 3171–3187.

Gautier-Soyer, M., Pollak, M., Henriot, M., Guittet, M.J., 1996. The (1×2) reconstruction of the α-Fe_2O_3 (-1012) surface. *Surf. Sci.* **352–354**, 112–116.

Halley, J.W., Rustad, J.R., Rahman, A., 1993. A polarizable, dissociating molecular dynamics model for liquid water. *J. Chem. Phys.* **98**, 4110–4119.

Henderson, M.A., 2002. Insights into the (1×1)-to-(2×1) phase transition of the α-Fe_2O_3(012) surface using EELS, LEED and water TPD. *Surf. Sci.* **515** (1), 253–262.

Henderson, M.A., Joyce, S.A., Rustad, J.R., 1998. Interaction of water with the (1×1) and (2×1) surfaces of α-Fe_2O_3(012). *Surf. Sci.* **417** (1), 66–81.

Henrich, V.E., Cox, P.A., 1994. *The Surface Science of Metal Oxides*. University Press, Cambridge.

Iordanova, N.I., Dupuis, M., Rosso, K.M., 2005. Charge transport in metal oxides: a theoretical study of hematite α-Fe_2O_3. *J. Chem. Phys.* **122**, 144305.

Jeon, B.-H., Dempsey, B.A., Burgos, W.D., 2003. Kinetics and mechanisms for reactions of Fe(II) with iron(III) oxides. *Environ. Sci. Technol.* **37**, 3309–3315.

Jones, F., Rohl, A.L., Farrow, J.B., van Bronswijk, W., 2000. Molecular modeling of water adsorption on hematite. *Phys. Chem. Chem. Phys.* **2**, 3209–3216.

Lad, R.J., Henrich, V.E., 1988. Structure of α-Fe_2O_3 single crystal surfaces following Ar^+ ion bombardment and annealing in O_2. *Surf. Sci.* **193** (1–2), 81–93.

Liger, E., Charlet, L., Van Cappellen, P., 1999. Surface catalysis of uranium(VI) reduction by iron(II). *Geochim. Cosmochim. Acta* **63** (19–20), 2939–2955.

Lloyd, J.R., Sole, V.A., Van Praagh, C.V.G., Lovley, D.R., 2000. Direct and Fe(II)-mediated reduction of technetium by Fe(III)-reducing bacteria. *Appl. Environ. Microbiol.* **66** (9), 3743–3749.

Lodziana, Z., Topsoe, N.-Y., Norskov, J., 2004. A negative surface energy for alumina. *Nat. Mater.* **3**, 289–293.

Madden, A.S., Hochella, M.F., 2005. A test of geochemical reactivity as a function of mineral size: manganese oxidation promoted by hematite nanoparticles. *Geochim. Cosmochim. Acta* **69**, 389–398.

Parker, S.C., deLeeuw, N.H., Redfern, S.E., 1999. Atomistic simulation of oxide surfaces and their reactivity with water. *Faraday Discuss.* **114**, 381–393.

Pedersen, H.D., Potsma, D., Jakobsen, R., Larsen, O., 2005. Fast transformation of iron oxyhydroxides by catalytic action of aqueous Fe(II). *Geochim. Cosmochim. Acta* **69**, 3967–3977.

Rustad, J.R., 2001. Molecular models of surface relaxation, hydroxylation, and surface charging at oxide–water interfaces. *Rev. Mineral. Gechem.* **42**, 169–197.

Rustad, J.R., Hay, B.P., Halley, J.W., 1995. Molecular dynamics simulation of iron(III) and its hydrolysis products in aqueous solution. *J. Chem. Phys.* **102**, 427–431.

Rustad, J.R., Wasserman, E., Felmy, A.R., 1999. Molecular modeling of the surface charging of hematite–II. Optimal proton distribution and simulation of surface charge versus pH relationships. *Surf. Sci.* **424** (1), 28–35.

Rustad, J.R., Felmy, A.R., Bylaska, E.J., 2003. Molecular simulation of the magnetite–water interface. *Geochim. Cosmochim. Acta* **67** (5), 1001–1016.

Rustad, J.R., Rosso, K.M., Felmy, A.R., 2004. Molecular dynamics investigation of ferrous–ferric electron transfer in a hydrolyzing aqueous solution: calculation of the pH dependence of the diabatic transfer barrier and the potential of mean force. *J. Chem. Phys.* **120** (16), 7607–7615.

Trainor, T.P., Chaka, A.M., Eng, P.J., Newville, M., Waychunas, G.A., Catalano, J.G., Brown, G.E., 2004. Structure and reactivity of the hydrated hematite (0001) surface. *Surf. Sci.* **573** (2), 204–224.

Wang, X.-G., Weiss, W., Shaikhutdinov, S.K., Ritter, M., Petersen, M., Wagner, F., Schlogl, R., Scheffler, M., 1998. The hematite (α-Fe_2O_3) (0001) surface: evidence for domains of distinct chemistry. *Phys. Rev. Lett.* **81**, 1038–1041.

Wasserman, E., Rustad, J.R., Felmy, A.R., Hay, B.P., Halley, J.W., 1997. Ewald methods for polarizable surfaces with application to hydroxylation and hydrogen bonding on the (012) and (001) surfaces of α-Fe_2O_3. *Surf. Sci.* **385** (2–3), 217–239.

Wasserman, E., Rustad, J.R., Felmy, A.R., 1999. Molecular modeling of the surface charging of hematite–I. The calculation of proton affinities and acidities on a surface. *Surf. Sci.* **424** (1), 19–27.

Waychunas, G.A., 1991. Crystal chemistry of oxides and oxyhydroxides. *Rev. Mineral.* **25**, 509.

Wiesendanger, R., Shvets, I.V., Coey, J.M.D., 1994. Wigner glass on the magnetite (001) surface observed by scanning–tunneling microscopy with a ferromagnetic tip. *J. Vac. Sci. Technol. B* **12**, 2118–2121.

Williams, A.G.B., Scherer, M.M., 2004. Spectroscopic evidence for Fe(II)–Fe(III) electron transfer at the iron oxide–water interface. *Environ. Sci. Technol.* **38**, 4782–4790.